*Tellus (2002), 54B, 22–40*
*Printed in UK. All rights reserved*


**TELLUS**
*ISSN 0280–6509*

# Long-range transport of carbon monoxide from tropical ground to upper troposphere: a case study for South East Asia in October 1997

By SHOICHI TAGUCHI[1]*, HIDEKAZU MATSUEDA[2], HISAYUKI Y. INOUE[2] and YOUSUKE SAWA[2], [1]*National Institute of Advanced Industrial Science and Technology, AIST Tsukuba West, 16-1 Onogawa, Tsukuba, Ibaraki, 305-8569, Japan;* [2]*Meteorological Research Institute, 1-1 Nagamine, Tsukuba, Ibaraki, 305-0052, Japan*

(Manuscript received 12 December 2000; in final form 10 September 2001)

ABSTRACT

High concentrations of carbon monoxide (CO) were observed in October 1997 at the upper troposphere of the western tropical Pacific. Transport from the potential sources of CO due to biomass burnings in the tropics was investigated by using a global chemical transport model (CTM) driven by assimilated meteorological data provided from European Centre for Medium-Range Weather Forecasts (ECMWF). A CTM evaluation simulation using water vapor showed that the amount of vertical transport of moisture by large-scale flow was consistent with the precipitation predicted at the convective zone. A series of CTM simulations using 10-day emission periods of an artificial material with lifetime of 60 days indicated that vertical lifting of surface air at the Indonesian archipelago occurred in the concentrated convections west of Sumatra Island. No evidence was found that CO from the Amazon region or Africa significantly contributed to high concentrations in the western tropical Pacific. Transport formed a large-scale anvil below the tropopause by rapid vertical transport and by divergence flow. The average time required for the transport from Kalimantan and Sumatra Island to the point of high CO concentration was about 15 days. High concentrations at an altitude of 10 km in the Southern Hemisphere were transported by large-scale subsidence from the upper tropospheric maximum, which was presumably produced from the sources at Kalimantan and Sumatra Island. Estimated emissions of CO in September and October from Kalimantan and Sumatra were substantially larger than the previous estimates. Omission of chemical reaction was a possible problem for the overestimate, but not significant. The possible problems in the transport were incorrect CTM transport due to insufficient horizontal ($2.5 \times 2.5^\circ$) and vertical resolution of the CTM, and to inaccuracy in the wind fields at the upper part of the troposphere and a divergent flow pattern in the upper part of the troposphere.

## 1. Introduction

Large-scale atmospheric motions in the tropical troposphere are characterized by the Hadley circulation and the Walker circulation. Latent heat release in the deep moist convections drives these circulations. Deep moist convection (horizontal scale of 1 km) is the only mechanism for upward transport in the tropics above the planetary boundary layer (PBL), and vertical transport integrated over certain large-scale areas (horizontal scale of 100 km) is related to large-scale convergence by cumulus parameterization in the

* Corresponding author.
e-mail: s.taguchi@aist.go.jp

numerical weather prediction model (Tiedke, 1989). Although large-scale meteorological data assimilated in forecast-analysis cycles might be sufficiently accurate to clarify the transport characteristics, Undén (1989) demonstrated that constraints in the assimilation, such as the magnitude of divergence, alters the direction and strength of assimilated winds significantly. By using assimilated winds, Newell et al. (1996) studied material transport in the Walker circulation and found that, based on the mass flux, rising motion in the western Pacific and sinking motion in the eastern Pacific are not linked. This contradicts the widely accepted view that such a connection exists. Using a global chemical transport model, Mahowald et al. (1997) showed substantial differences in transport characteristics for assimilated meteorological data from two projects, namely the European Centre for Medium-Range Weather Forecasts (ECMWF) and National Center for Environmental Prediction (NCEP). Limitations of the application of assimilated wind fields need to be determined for the study of atmospheric transport.

Carbon monoxide (CO) is an essential, minor constituent in the atmosphere, because it can alter the atmospheric oxidizing capacity, not only in urban areas but also in remote, non-industrial areas. The oxidizing capacity in the troposphere is determined mainly by the amount of hydroxyl radical (OH). Because CO acts as a major sink of OH, which influences atmospheric concentrations of greenhouse gases such as methane and replacements for chlorofluorocarbons, global emissions of CO into the atmosphere directly affect the chemical composition of the atmosphere, and therefore indirectly affect the climate of the Earth. Using a transport model, Bergamaschi et al. (2000) estimated emission scenarios to be 643–872 TgC/yr from technological emissions, 139–459 TgC/yr from isoprene, 554–771 TgC/yr from forest biomass, and 642–847 TgC/yr from methane oxidation. Crutzen and Andreae (1990) estimated the emission of CO from tropical biomass-burning to be 120–510 TgC/yr, a range that includes interannual variability as well as uncertainty in the estimate of the source strength. Geographical distributions of biomass burnings in the tropics were discussed by Andreae (1991) and by Hao and Liu (1994).

A large part of the removal of CO is caused by reactions with OH. The reaction rate of CO + OH is $1.5 \times 10^{-13}$ $(1 + 0.6P/101\,325)$ (DeMore et al., 1997), where $P$ is the atmospheric pressure in Pa. Concentrations of monthly mean OH in the tropics range from $5 \times 10^5$ to $20 \times 10^5$ molecules/cm$^3$ (Spivakovsky et al., 2000). This range suggests that the lifetime of CO is 23–92 days at the surface and 33–134 days at an altitude of 10 km.

The purpose of our current study was to use a three-dimensional (3-D) numerical model to quantify the influence of biomass burning on CO enhancement in regions of southeast Asia during October 1997. Extensive and widespread vegetation and peat fires occurred in Kalimantan and Sumatra, Indonesia, from August 1997 to March 1998. Using satellite data, Gutman et al. (2000) demonstrated an impact of El Niño on Kalimantan Island. Large-scale circulations were studied by Kita et al. (2000) who suggested that an updraft west of Sumatra Island significantly affected the vertical transport in October 1994 and 1997. Anomalies in the large-scale circulation in the tropics in October 1997 were demonstrated by the precipitation record in East Kalimantan (Toma et al., 2000). This reduction in recorded precipitation caused a drought on Kalimantan and contributed to extensive forest and peat fires. From late September to early December 1997, an air-sampling project by commercial aircraft revealed greatly enhanced concentrations of CO ($\sim$380 ppb) in the upper troposphere over the western Pacific (Matsueda and Inoue, 1996; Matsueda et al., 1998; Matsueda et al., 1999). This concentration exceeded the surface CO concentrations down-wind of India in winter (Lelieveld et al., 2001). These high concentrations coincided with the increased biomass burnings in Sumatra and Kalimantan in 1997, although the source of CO from biomass burning in the southern subtopics was attributed to possible long-range transport (Matsueda et al., 1999). Andreae (1991) showed that large sources of CO due to biomass-burnings were also present in the Amazon region and in Africa. Aerosol concentrations derived from satellite imaging were high over New Guinea (Nakajima et al., 1999), and the level of haze at the surface was also high (Maiha, 1998), indicating the existence of smoldering biomass-burning. Tropospheric ozone was also enhanced during this period (Thompson et al, 2001).

First, we show temporal data of CO concentra-

tions in the upper troposphere measured from 1993 to 1998. Then, we show meteorological conditions in October 1997, focusing on moisture and precipitation. Next, we show results of 3-D numerical simulations of moisture, pulse input of markers from potential sources in the Tropics, and continuous emissions of CO reacting with monthly and zonally averaged OH fields. Finally, we show our estimation of emission strength based on measured CO.

## 2. Airborne CO measurements and mean meteorological fields

CO measurements were made twice a month from a passenger aircraft flown from Australia to Japan. Figure 1 shows monthly mean CO concentrations measured at altitudes of 8–13 km over the western Pacific in the Northern and Southern Hemispheres from 1993 to 1998. Although detailed temporal and spatial variations were already reported up to 1997 by Matsueda et al. (1999), new data taken in 1998 are also shown to present a more long-term record. Details of the sampling

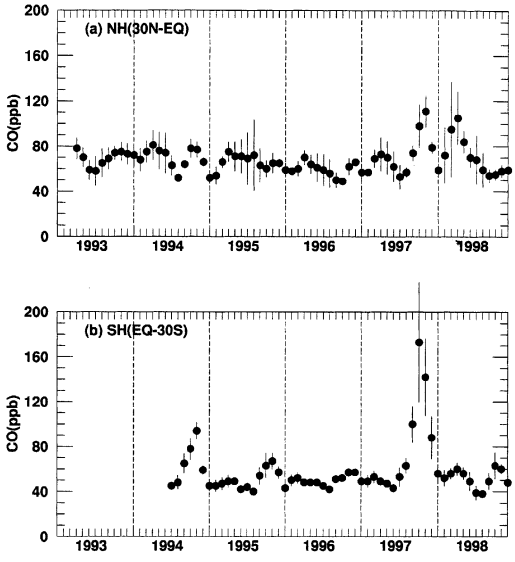


*Fig. 1.* Monthly mean CO concentrations in the Northern Hemisphere between 30°N and the equator (a), and the Southern Hemisphere between the equator and 30°S (b) observed at altitudes of 8–13 km over the western Pacific from 1993 to 1998. Error bars are ±1 standard deviation of the mean.

positions and altitudes were described by Matsueda et al. (1999).

In the Southern Hemisphere, the CO showed a large inter-annual variation from 1993 to 1998, and showed a distinct peak in October 1997. A similar seasonal peak appeared in 1994 and 1995, but was smaller than that in 1997. In the Northern Hemisphere, the CO concentration in 1997 also showed a clear increase near October. This enhanced CO level sharply decreased at the end of 1997, but again increased during March and April of 1998.

Measurements on 14 October 1997 are listed in Table 1 and on 28 October in Table 2, although the results of the simulation will be discussed in Section 3.4. Maximum concentrations were 291 ppb on 14 October at 18.3°S and 381 ppb on 28 October at 15.7°S. Minimum concentrations were observed over the Equator on 14 October and 12.3°N on 28 October.

Figure 2 shows the air-sampling locations during two flights in October 1997. Pressure level of 250 hPa is the nearest level to the sampling altitude. (The maximum departure of sampling location from 250 hPa altitude was about 1.5 km.) Streamlines drawn from monthly mean horizontal wind at 250 hPa indicate that air along the flight path came from several sources. Contributions from different sources also occur from rising motion in the Northern Hemisphere and sinking motions in the Southern Hemisphere, as will be shown in Section 3.3. Note that air at around 20°S came from air of the far west, beyond the region shown in this chart.

Figure 3 shows the mixing ratio of water vapor at 250 hPa as a monthly mean value. The mixing ratio is conserved during the transport if no condensation or evaporation occurred. Vertical motions and relative humidity (not shown) had horizontal distributions similar to the water vapor mixing ratio, indicating that rising motions transports moisture from lower layers to upper layers. This figure shows a moist band from the northern edge of Sumatra Island to the Philippine Islands. This band corresponds to a branching zone in streamlines seen in Fig. 2. A steep north–south gradient in moisture occurred along the equator over the Indonesian archipelago, indicating that the air masses on either side of the equator differ in origin. South of 10°S, west of Australia, was occupied by dry air, indicating that the area was

Table 1. *Observed concentrations of CO (ppb) and simulated concentration at sampling locations on 14 October 1997*

| Time (h:min) | Lat. (°N) | Long. (°E) | Height (km) | CO (ppb) | Kali. (ppb) | Sumat. (ppb) | New G. (ppb) | Aust. (ppb) | Amaz. (ppb) | Afri. (ppb) |
|---|---|---|---|---|---|---|---|---|---|---|
| 8:02 | 31.4 | 140.6 | 10.7 | 105 | 30.1 | 34.7 | 7.6 | 20.6 | 19.8 | 13.7 |
| 7:21 | 26.0 | 141.8 | 10.7 | 175 | 69.4 | 64.8 | 31.2 | 36.1 | 11.8 | 11.5 |
| 6:40 | 20.6 | 143.2 | 10.7 | 147 | 77.1 | 66.3 | 31.6 | 39.0 | 9.7 | 10.9 |
| 5:59 | 15.3 | 144.1 | 10.7 | 64 | 47.2 | 40.6 | 30.8 | 29.0 | 8.7 | 12.3 |
| 5:17 | 9.9 | 143.1 | 10.7 | 67 | 27.2 | 25.2 | 24.7 | 20.4 | 8.1 | 11.1 |
| 4:36 | 4.5 | 144.0 | 10.7 | 64 | 20.5 | 16.9 | 607.3 | 35.3 | 8.1 | 12.9 |
| 3:55 | −1.3 | 144.0 | 9.4 | 120 | 25.2 | 20.4 | 544.1 | 36.6 | 9.3 | 15.1 |
| 3:14 | −7.1 | 144.2 | 9.5 | 201 | 34.9 | 31.1 | 446.1 | 36.1 | 12.1 | 20.3 |
| 2:33 | −12.8 | 145.1 | 9.5 | 132 | 76.9 | 84.3 | 62.6 | 41.7 | 20.0 | 22.0 |
| 1:52 | −18.3 | 146.3 | 9.5 | 291 | 96.1 | 110.4 | 27.2 | 48.6 | 27.2 | 21.2 |
| 1:11 | −23.7 | 148.0 | 9.5 | 194 | 65.1 | 76.5 | 16.6 | 37.3 | 38.1 | 31.0 |
| 0:29 | −29.1 | 149.5 | 9.5 | 122 | 26.5 | 31.4 | 6.3 | 20.9 | 41.6 | 50.0 |

Measurement time in hour and minutes in Universal Time Coordinated together with latitude, longitude and height in km and measured CO concentration in ppb are listed in the left half. Measured values are provisional. Values are subject to future revisions. In the right half of the table, simulated concentrations from constant and continuous emissions from six potential sources in the Tropical land area are listed. Locations of source are Kalimantan, Sumatra, New Guinea, Northern Australia, Amazon and Africa. Details of the experiment are discussed in Section 3.4.

Table 2. *Same as Table 1 except for 28 October 1997*

| Time (h:min) | Lat. (°N) | Long. (°E) | Height (km) | CO (ppb) | Kali. (ppb) | Sumat. (ppb) | New G. (ppb) | Aust. (ppb) | Amaz. (ppb) | Afri. (ppb) |
|---|---|---|---|---|---|---|---|---|---|---|
| 8:17 | 33.9 | 140.0 | 9.6 | 117 | 20.7 | 21.0 | 3.5 | 14.0 | 13.2 | 12.3 |
| 7:36 | 28.6 | 141.3 | 10.7 | 112 | 59.3 | 31.5 | 39.1 | 27.5 | 12.0 | 12.3 |
| 6:55 | 23.2 | 142.5 | 10.7 | 85 | 28.6 | 24.7 | 22.9 | 21.7 | 9.2 | 11.0 |
| 6:14 | 17.9 | 144.4 | 11.3 | 70 | 24.8 | 25.2 | 21.6 | 19.1 | 9.4 | 11.3 |
| 5:33 | 12.3 | 145.0 | 10.7 | 69 | 22.9 | 22.2 | 22.8 | 18.6 | 7.9 | 10.1 |
| 4:52 | 6.8 | 145.5 | 10.7 | 103 | 18.3 | 17.4 | 43.4 | 16.5 | 6.7 | 9.8 |
| 4:11 | 1.2 | 146.0 | 10.7 | 227 | 16.1 | 15.2 | 517.5 | 23.6 | 7.1 | 13.1 |
| 3:30 | −4.4 | 146.6 | 10.7 | 86 | 15.2 | 14.7 | 527.7 | 21.7 | 7.5 | 14.5 |
| 2:49 | −10.0 | 147.3 | 10.1 | 93 | 54.4 | 61.7 | 26.9 | 34.6 | 24.4 | 17.0 |
| 2:08 | −15.7 | 148.2 | 10.1 | 381 | 75.6 | 85.9 | 23.8 | 46.6 | 30.0 | 18.4 |
| 1:27 | −21.5 | 149.0 | 10.1 | 342 | 73.8 | 80.7 | 28.0 | 46.3 | 32.4 | 18.8 |
| 0:44 | −27.6 | 149.6 | 10.1 | 118 | 41.2 | 50.5 | 7.3 | 73.3 | 55.6 | 42.6 |

covered by sinking motion. Note that air south of the equator at 250 hPa was supplied from upper levels, rather than from horizontal transport or upward transport directly from the ground.

## 3. Chemical transport model experiments

### *3.1. Model description*

The Chemical Transport Model (CTM) used in this study (NIRE-CTM-96) was developed at the National Institute for Resources and Environment (NIRE). Meteorological data (provided by the ECMWF) in 1997 were used to drive the transport calculations. In the NIRE-CTM-96 model, the CO concentrations were calculated at regular grid points of $2.5^\circ \times 2.5^\circ$ longitude–latitude distances. The number of vertical levels was 15, consisting of 0.99 and 0.925 sigma coordinates in the lowest two atmospheric levels, four hybrid coordinates in the intermediate levels, and nine pressure coordinates in the upper part atmosphere (300, 250, 200, 150, 100, 70, 50, 30, 10 hPa). Concentrations

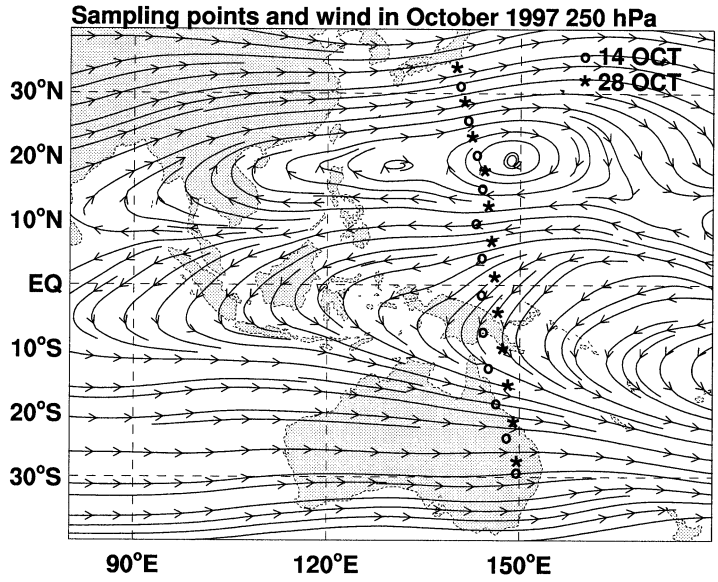


*Fig. 2.* Air-sampling locations for two flights and monthly mean wind at 250 hPa in October 1997. Sampling locations are indicated by circles (14 October) and asterisks (28 October). Altitude (km) of sampling locations are also shown. Horizontal winds are ECMWF analysis.

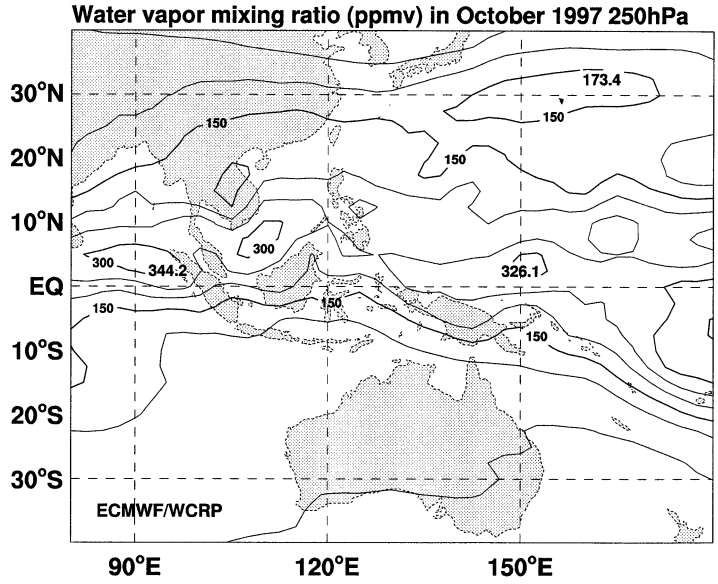


*Fig. 3.* Water vapor mixing ratio (ppmv) at 250 hPa averaged October 1997 (ECMWF/WCRP). Contours are in intervals 50 ppmv.

of water vapor, artificial material and CO at 6-h intervals were calculated. Meteorological data were provided at 6-hr intervals over the entire world with $2.5^\circ \times 2.5^\circ$ horizontal resolution and at 15 pressure levels. Advection was calculated by using a 3-D semi-Lagrangian scheme. In this scheme, the hmixing ratio at a regular point is considered identical to the mixing ratio 6 h upstream from that regular point. We call it a departure point. The mixing ratio at the departure point is estimated from those at the regular grid surrounding the departure point. We call this volume surrounded by eight regular grids a cage. The departure point was estimated by back trajectory analyses from the regular point using 3-D wind fields.

Either a 3-D linear interpolation or nearest grid-point-value method was used to estimate the concentration at the departure point off the regular grid. The nearest grid-point value was used when a cage outside the tropics (north of 30°N and south of 30°S), was intersected by tropopause. Intersection was defined as when the tropopause pressure is the same or larger than the pressure of the top boundary of the cage and smaller than the pressure of the bottom boundary of the cage. In the Tropics (30°S to 30°N), both methods were used consecutively. Horizontal linear interpolation was done and then the value at the nearest vertical level was selected even if the tropopause intersected a cage. A linear interpolation is used in a cage without a tropopause. A thermal tropopause (Hoinka, 1998) was used to determine the pressure of the tropopause with a critical lapse rate of 13 K/km for potential temperature.

The nearest grid-point-value method reduced the troposphere–stratosphere exchange rate. For stratospheric air, due to the reduction of the exchange rate, turn-over time was elongated from 0.5 yr in NIRE-CTM-93 (full linear interpolation model) to 1.8 yr in the current model. For tropospheric air, the reduction of stratosphere–troposphere exchange rate produced a realistic semi-rigid top.

The total mass of a constituent was conserved by using a mass-fixing procedure in which the concentrations were adjusted to maintain a constant global amount before and after the transport (Taguchi, 1996, Appendix). A major deficiency of this procedure, however, was that the additive nature did not hold when multiple sources (were present, because adjustments occurred in different locations for each case. This slightly affected the source estimate but did not significantly alter conclusions inferred from this research.

The algorithm used to calculate the change in concentrations due to turbulent mixing functioned as follows. Turbulent mixing was calculated only in the levels below the top of the PBL. The altitude of the model PBL was estimated from the bulk Richardson number. The temperature at an altitude of 2 m was used to calculate the bulk Richardson number. During a CTM time-step, materials in model layers within the PBL were redistributed among the layers in the PBL to make a uniform concentration. PBL reached 1–2 km altitude at 06 UTC over the Indonesian archipelago, and remained at the lowest single level at other times. The central pressure between the lowest layer and the second lowest layer was always used for the pressure of the top of the PBL when the PBL altitude was lower than that level. Therefore accumulation of constituents in nocturnal stable layers is possibly underestimated. Note that the CTM considered the expansion of the PBL due to dry and wet convection during the daytime, and mechanical mixing due to high wind speeds. Additional details of the semi-Lagrangian scheme, mass preserver, and PBL were described by Taguchi (1996).

### 3.2. *Model verification*

The basic performance of NIRE-CTM-96 was demonstrated in previous inter-comparison experiments reported by Denning et al. (1999). We evaluated global transports of the NIRE-CTM-96 by using $SF_6$ and $CO_2$ (Rayner and Law, 1995; Denning et al., 1999). We also evaluated regional transport by using published data of Radon-222 over Moffett fields (Kritz et al., 1998), TROPOZ-II (Ramonet et al., 1996), and NARE (Zaucker et al., 1996). Results of NIRE-CTM were similar to other models such as TOMCAT (Stockwell et al., 1998), MATCH (Mahowald et al., 1997) and TM3 (Dentener et al., 1999).

Because no radon data are available for the Indonesian area in October 1997, we used alternative available data. Here we describe a method to verify large-scale transport using water vapor and precipitation. Moist cumulus convection lifts materials from the ground layers into the upper

tropical atmosphere. In a global chemical transport model, with horizontal grid scales over 100 km and time resolution more than a hour, micro-scale information (of the order of 1 km) on the transport by moist convection is lost. Unfortunately, inferring how much is missing is not straightforward, because during moist convection the transport is asymmetric, with a sinking motion occupying most of the region, and the rising motion confined to a narrow sub-region. Inferring micro-scale information is further complicated because the numeral weather prediction (NWP) model which supplies pseudo-observations for an area of no observations already accounts for the flux due to the cloud ensemble, including penetrative convection (Tiedke, 1989). In the data assimilation process, predictions of wind fields from NWP and observations are mixed to form a meteorological field on regular grid points.

Equations expressing large-scale moisture transport in NWP are in the form

$$\frac{\partial \bar{q}}{\partial t} + \bar{\boldsymbol{v}} \cdot \nabla \bar{q} + \bar{w} \frac{\partial \bar{q}}{\partial z} = -\frac{1}{\bar{\rho}} \frac{\partial}{\partial z} (\overline{\rho w' q'}) - (\bar{c} - \bar{e}) \quad (1)$$

where $q$ is the specific humidity, $\rho$ is the density of the air, $\boldsymbol{v}$ is the horizontal velocity, $w$ is the vertical velocity, $c$ is the rate of condensation, $e$ is the rate of evaporation and the prime denotes deviations from the horizontal average (Tiedke, 1989). Suspended water in the form of liquid, such as rain droplets or cloud droplets, is not included in the transport represented in eq. (1). Cumulus parameterizations are used to describe the first term on the right-hand side of eq. (1). The net precipitation can be calculated by integrating eq. (1) vertically as

$$\int_{\text{bottom}}^{\text{top}} (\bar{q}_{\text{o}} - \bar{q}_{\text{m}})\, \mathrm{d}z = C - E \quad (2)$$

where $q_{\text{o}}$ is the observed mixing ratio, $q_{\text{m}}$ is the prediction of water vapor mixing ratio in the CTM, $C$ is the surface precipitation, and $E$ is the evaporation. Eddy flux terms are eliminated by assuming that the eddy fluxes at the top and bottom of the atmosphere are both zero. Due to the absence of the eddy flux term, the performance of the CTM for large-scale circulations can be evaluated without considering eddy terms. The right-hand side is taken from the ECMWF data set, which provides precipitation and evaporation data integrated in the forecast (12–36 h). We used these forecast values as observed precipitation data because the predictions were made by using a higher resolution atmospheric model and were tested against observed rainfall data (Gregory et al., 1998). NIRE-CTM-96 predicted the difference between condensation and evaporations at 6-h time intervals from an initial distribution of water vapor at each time step. Note that precipitation does not verify subgrid scale mixing.

Figure 4 shows monthly averages of precipitation and evaporation during October 1997. The upper panel is the sum of ECMWF forecast fields of sub-grid scale (convective) precipitation, grid scale (large scale) precipitation and evaporations. The lower panel shows the NIRE-CTM integrations. Locations of heavy rain in the ECMWF analysis (west of Sumatra Island and north of the equator near New Guinea) are consistent with the wet area shown in Fig. 3. Heavy rains over Mindanao and New Guinea were not observed in moisture fields at 250 hPa, probably because the precipitation there was sporadic, or because outflow from the cloud might occur in lower altitudes.

South of the equator at the Indonesian archipelago was covered by a no-rain area. The rain area extended down to 10°S in non-El Niño years (not shown). Note that during those years pollutants emitted from the ground were transported effectively to the upper troposphere.

Precipitation from the ECMWF/WCRP forecasts for New Guinea, the northern part of Kalimantan Island and west of Sumatra Island was reproduced well by using the NIRE-CTM. Precipitation areas in the Indian Ocean as well as the Pacific Ocean in ECMWF were also reproduced well by using the NIRE-CTM. Absolute magnitudes were higher by using the NIRE-CTM, probably because liquid water suspended in the air was not excluded from precipitation estimated with the NIRE-CTM.

Figure 5 shows a comparison of the daily precipitation levels west of Sumatra (95°E, 2.5°N) where the peak monthly precipitation was observed. Precipitation varied with time and was largely determined by the vertical motion in the middle of the troposphere. Daily rain estimated using the NIRE-CTM was consistent with that from the ECMWF/WCRP forecasts, although a shift in the event, of the order of one day, was occasionally observed (e.g., 14 and 27 October).

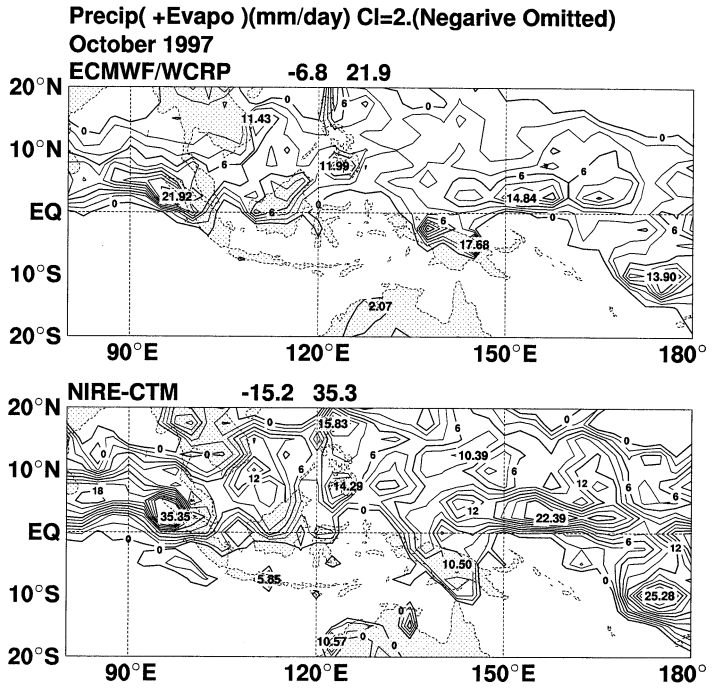


*Fig. 4.* Monthly precipitation (mm/day) during October 1997. (a) ECMWF predictions. Average of 24-h between 12 and 36 h after the start of NWP. (b) Average precipitation at 6-h intervals estimated from NIRE-CTM-96. Units mm/day. Contour interval 2 mm/day.

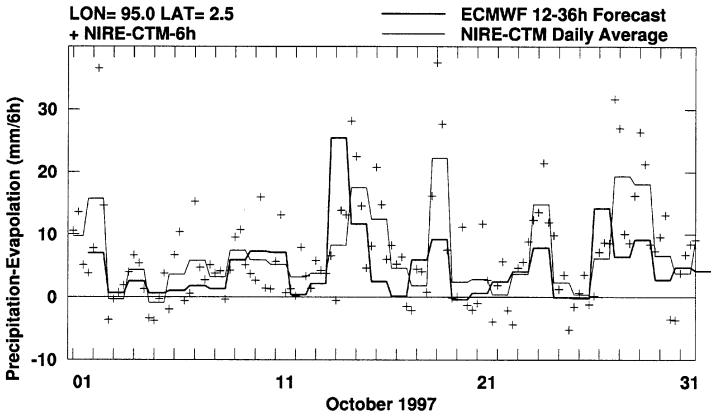


*Fig. 5.* Daily precipitation in October 1997 at 95°E, 2.5°N. Precipitation of ECMWF forecasts (thick line) and NIRE estimates (thin line for daily mean and crosses for 6-h intervals).

### *3.3. Pulse emission experiment*

To investigate transport timescales, we input the short-term emissions of a marker with a lifetime of 60 days, like a dye in a fluid-dynamics laboratory experiment, into the CTM. This marker, initially with zero concentrations everywhere, was simulated for 4-month periods. Emissions were active only for the first 10 days. By pulsing the emissions on and off, we could monitor the following parameters: (1) locations of lifting points for a particular surface source, (2) the

relative strength of diffusion in upper atmospheric levels and surface levels, (3) the timescale for arrival of the marker and (4) contributions of air mass from each source to air-sampling sites. Six simulations were done for each source from September to October 1997, such that the first simulation started on 1 September, the second started on 11 September, and so on.

Andreae (1991) and Hao and Liu (1994) reported that major source regions of tropical biomass burnings were southeast Asia, southern Africa, South America, and northern Australia. Therefore, in our numerical simulations we used the six source regions shown in Fig. 6. The emission points (×) were placed at two grid points over Kalimantan, Sumatra, New Guinea and northern Australia. Nine emission points were placed over Africa and the Amazon. The total amount of emission for each area was 500 TgC/yr, which was near the maximum estimate of CO for total topical biomass burnings reported in the literature (Crutzen and Andreae, 1990).

Figure 6 also shows lifting points for each source. Lifting points were defined as the grid points where concentrations first exceeded 10 ppb at 250hPa. In the tropics, rising motions were confined to such a lifting tower. Sumatra (b), New Guinea (c) and Africa (e) sources had lifting points close to the emissions. Kalimantan (a) source had lifting points relatively far from the emission points. Northern Australian (d) and Amazonian (f) sources had no lifting points within a few hundred km from the emission points. Note that the sources at Sumatra, Kalimantan and northern Australia shared the same lifting tower at certain times during the study period, indicating the difficulty in distinguishing the source from the distribution of concentrations in the upper troposphere.

Figure 7 shows a composite of the six time series of horizontal sizes, defined as the area exceeding 10 ppb of marker at 250 hPa and 0.99 sigma levels for six individual sources. Solid lines represent mean values for each time step, and thin lines represent $\pm 1$ standard deviation (for six cases here) from the mean. Three areas in the left panels (a, b and c) had a common feature that upper tropospheric expansion was larger than that at the surface. This expansion was analogous to an anvil of deep cumulus convections, and was also related to the upper tropospheric maximum (UTM) (Jonquieρes and Marenco, 1998). Also note that maximum concentrations were located at altitudes higher than 250 hPa at 145°E (not shown).

The size of the area in the upper troposphere over northern Australian sources was comparable to those at lower levels. The time lag between the occurrence of peak size in surface level and upper troposphere was about 20 days. This delay was consistent with the distances between the source and lifting points (Fig. 6). The areas in the surface level and the upper troposphere from the African source were similar to those from the Amazonian source, indicating that vertical transport was inactive at that location and time.

Figure 8 shows a composite of the six time series of the concentrations at a single receptor point (145°E, 17.5°S, 250 hPa) for each of the six source areas. This point was selected to demonstrate the delay time for transport from an equatorial source to the subtropical upper troposphere. Furthermore, the point was located near the sampling point where the maximum concentrations were observed. The abscissa represents the starting time of the emission at each source.

The time required to reach the receptor from the source was more than 15 days after the start of the numerical simulations. Maximum concentrations occurred even later, from 20 days for Sumatra to 33 days for northern Australia. This longer time can be explained by the distances of the lifting points from the sources shown in Fig. 6. For New Guinea (c), the time evolutions of the concentrations varied for each set of simulations, resulting in a large standard deviation.

### 3.4. *Continuous emission experiment*

Relative contributions of CO in the upper troposphere were evaluated using continuous, constant-rate CO emissions from six potential sources given in Fig. 6. The CO calculation was initialized on 1 January 1997, with no CO at any grid point. The model was run until October 1997. Simulations were done independently for each emission region. Because the oxidative reaction with OH is a dominant sink for tropospheric CO, we used monthly and zonally averaged OH distributions (Spivakovsky et al., 2000).

Figure 9 shows horizontal distributions of CO at 250 hPa at 06 UTC on 14 October 1997. CO

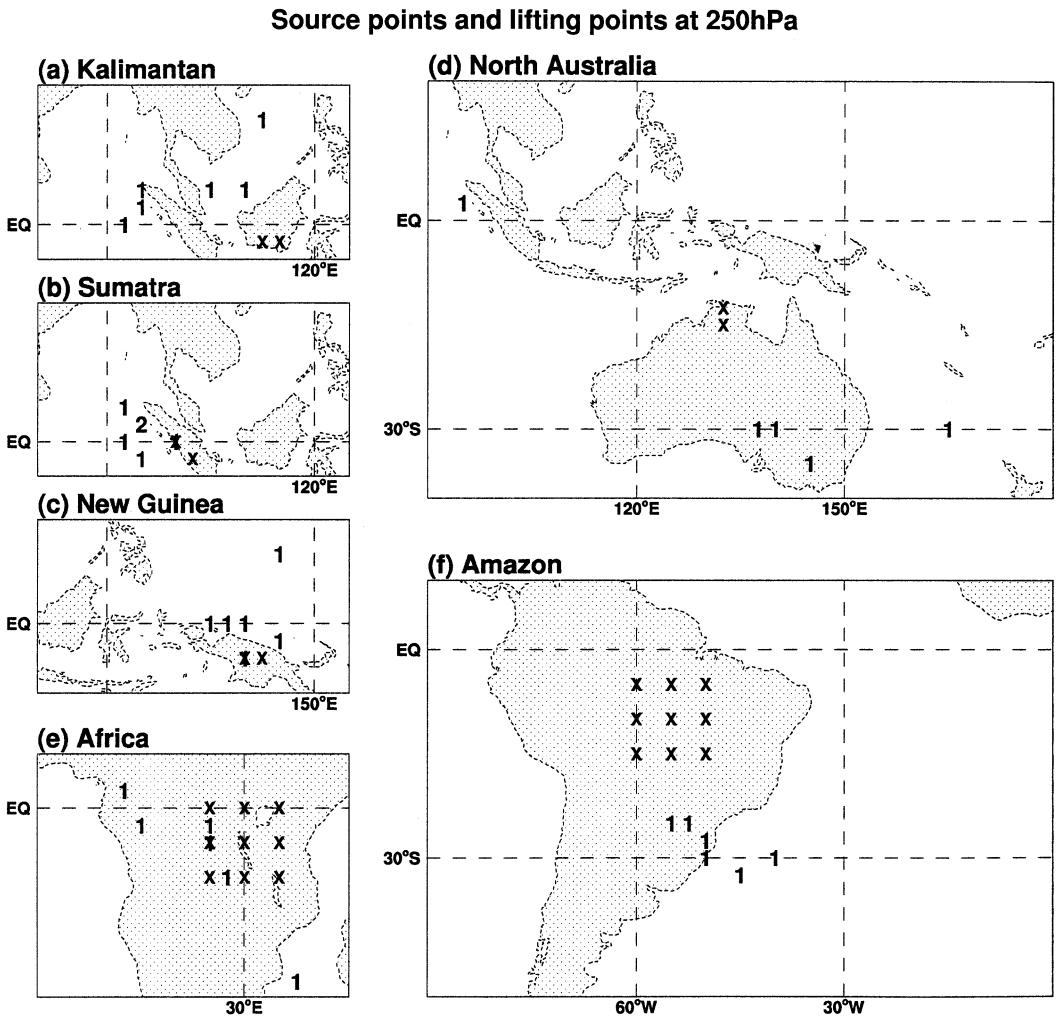


*Fig. 6.* Emission and lifting points. Kalimantan (a), Sumatra (b), New Guinea (c), northern Australia (d), Africa (e) and the Amazon (f). Two emission points marked by (×) were given to (a), (b), (c) and (d). Six emission points were given at (e) and (f). Each emission area was normalized to give 500 TgC/yr emission. Lifting points (marked by 1 or 2) were defined as grid points on which concentrations at 250 hPa first exceeded 10 ppb. The frequencies of the occurrence of lifting points among the six simulations are shown. One point in (c) is outside of the figure area.

from Kalimantan Island (a) forms a unique distribution pattern. The flow of CO at 100°E on the equator divides into three branches, although high concentrations do not appear just above the source point of Kalimantan. One branch extends west along the equator from Sumatra to the African continent through the tropical Indian Ocean. The second branch extends west along a path 20–30°N to subtropical north Pacific regions, through southern Japan. The third branch passes over mid Australia to the subtropical South Pacific along a path 20–30°S.

CO from Sumatra (b) shows a similar distribution pattern to that from Kalimantan, because the CO distribution shows three main flows separated at 100°E on the equator. CO from New Guinea (c) shows a different distribution pattern, although New Guinea is close to Kalimantan. High CO

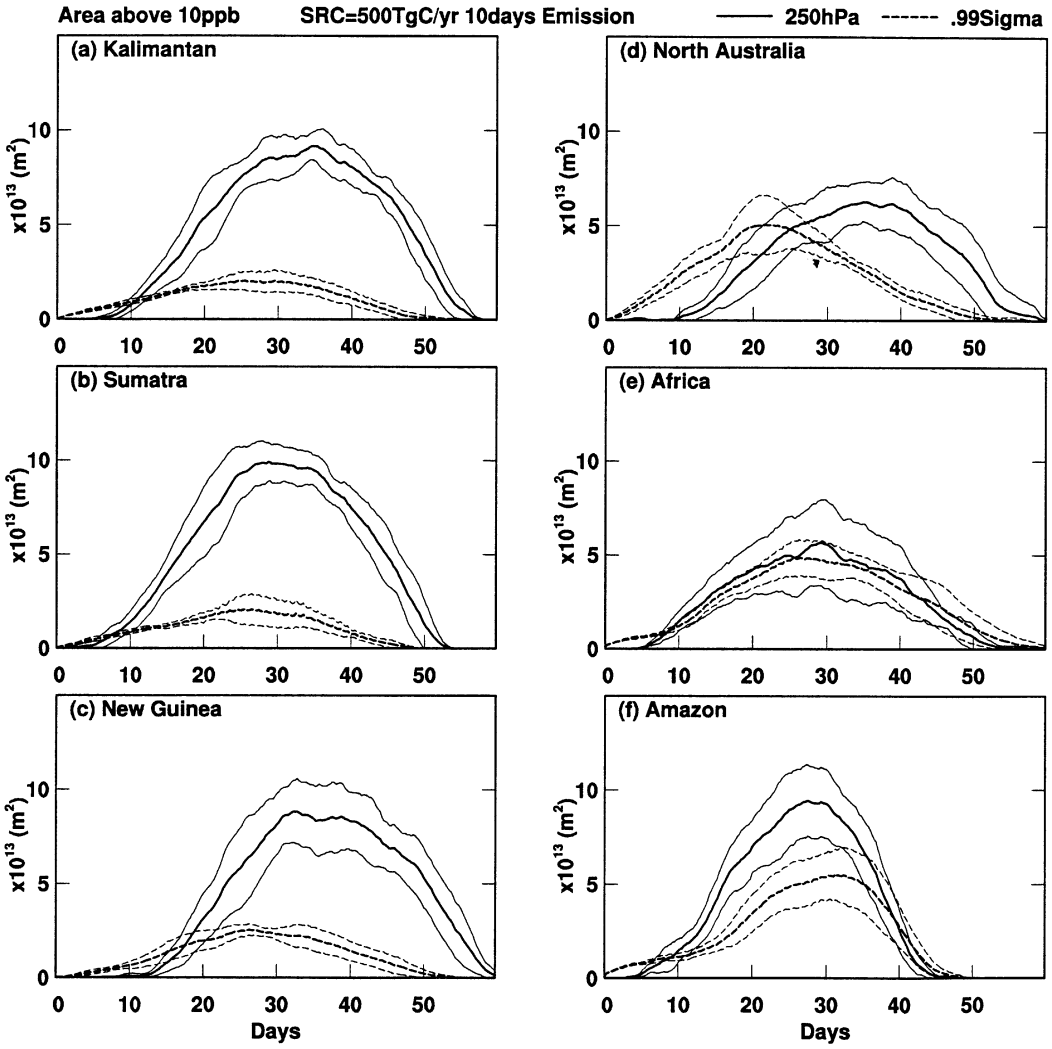


*Fig. 7.* Simulated CO concentrations higher than 10 ppb as a function of time. Kalimantan (a), Sumatra (b), New Guinea (c), northern Australia (d), Africa (e) and the Amazon (f). Composite of six simulations. Concentration at 250 hPa is indicated by the thick line, and that at the surface by the thick dotted line. Thin lines show 1 standard deviation of six concentrations.

branches are observed over the Philippine Islands to the mid-south Pacific. High concentrations above New Guinea Island indicate rapid lifting by strong vertical winds and less horizontal transport in the upper layer.

CO from northern Australia (d) shows a distribution pattern similar to those from Sumatra and Kalimantan, but the concentrations were lower than those from Indonesian sources. High CO concentrations did not appear just above the source point of northern Australia, because the released CO was rapidly transported toward Sumatra by the prevailing surface wind and then was lifted at 100°E in the equatorial region. As a result of this long travel in the surface air, the CO concentration was reduced by aging.

CO from Africa (e) formed high concentrations over the source, and then separated at 250 hPa to

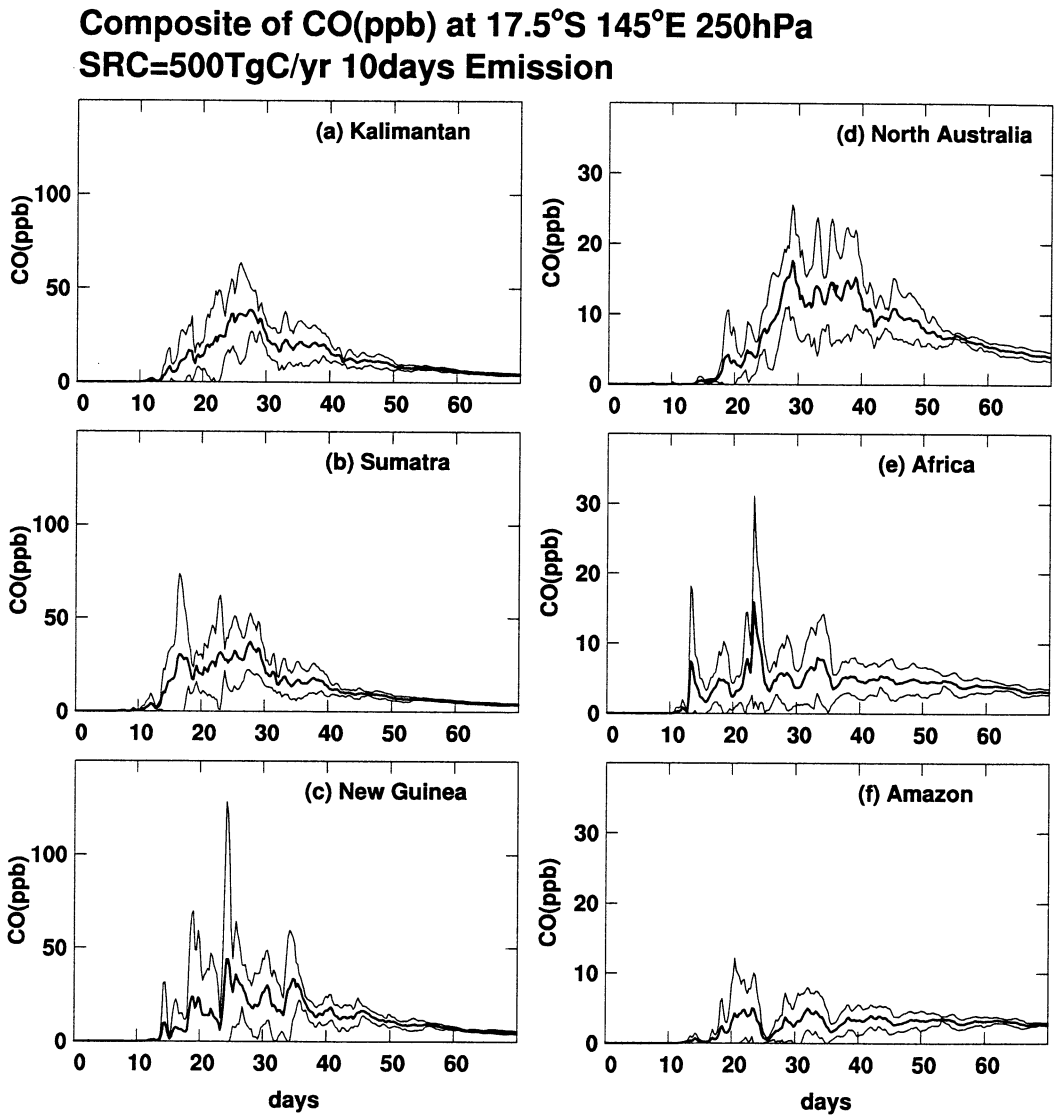


*Fig. 8.* CO concentrations at 145°E, 17.5°S, 250 hPa for source emission from Kalimantan (a), Sumatra (b), New Guinea (c), northern Australia (d), Africa (e) and the Amazon (f). Composite of six simulations. Thick line indicates the mean concentration, and thin lines indicate 1 standard deviation of six concentration.

the west and to the east. The CO to the west spread to South America through the tropical Atlantic Ocean, whereas the CO to the east was transported to mid Australia across the South Indian Ocean. For the CO from Kalimantan and Sumatra, a filament with high concentrations over eastern Australia appeared in the mid-latitudes south of 30°S, transport behavior that was different from the southern subtropical branch near 20°S. CO from the Amazon region (f) passed through the middle latitudes in the Southern Hemisphere south of 30°S, where high concentration areas appeared. The CO concentrations over eastern Australia from the Amazon were similar to those from Africa. In the Northern Hemisphere, no significant intrusion of CO was found from

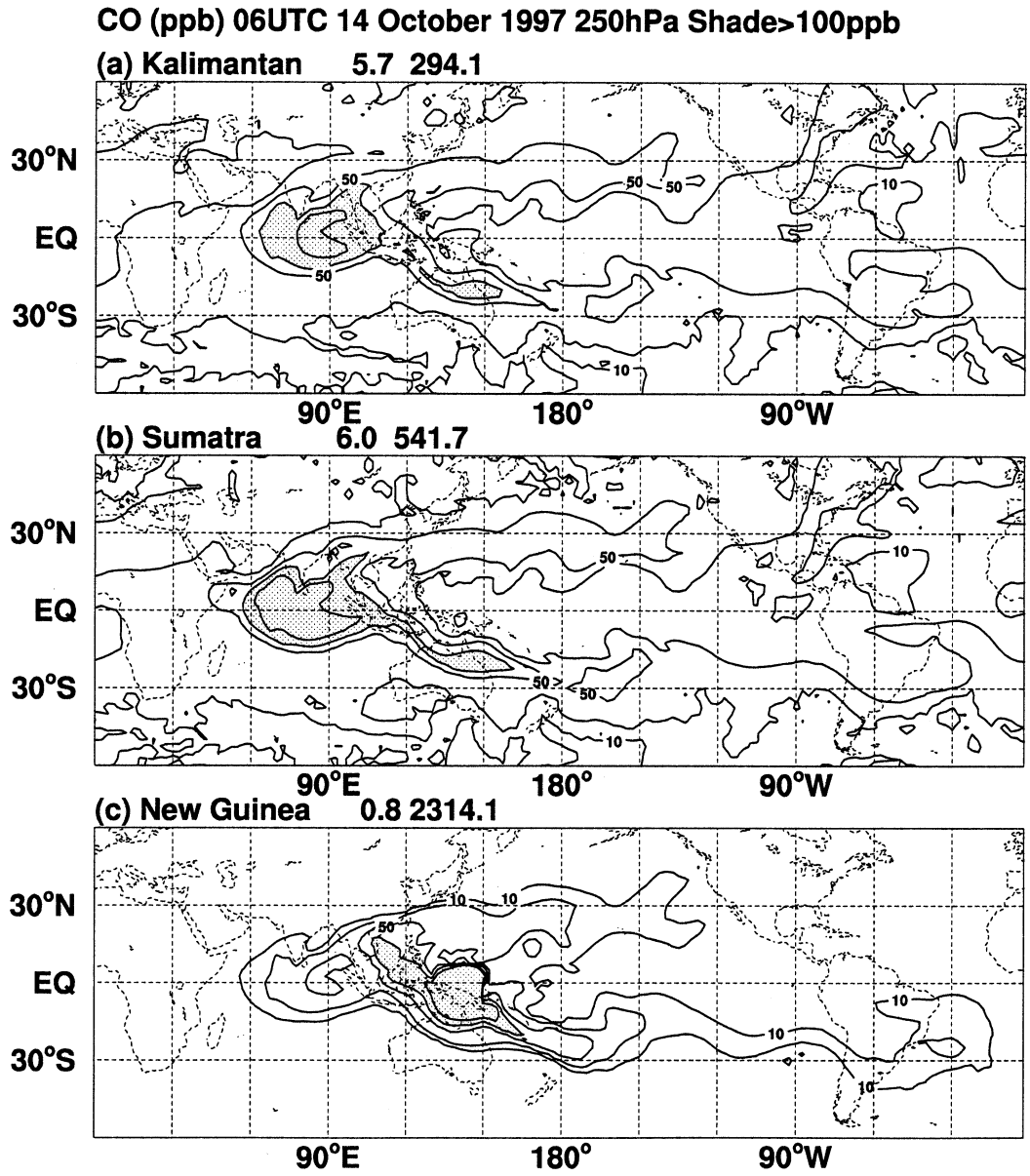


either the Amazon region or from Africa, although as previously stated, significant transport of CO from southeast Asia to the northern subtropics was found. These observed characteristic features were also reproduced in the CO distribution pattern simulated with the 3-D numerical model with combined biomass-burning emissions from the Amazon and Africa (Allen et al., 1996).

### 3.5. *Emission estimate*

To estimate the CO emissions from biomass burning in southeast Asia during October 1997, we used a simple parameter fitting method, technically called systematic exploration of model space (Tarantola, 1987). This method evaluates a degree of fitting between observed and simulated

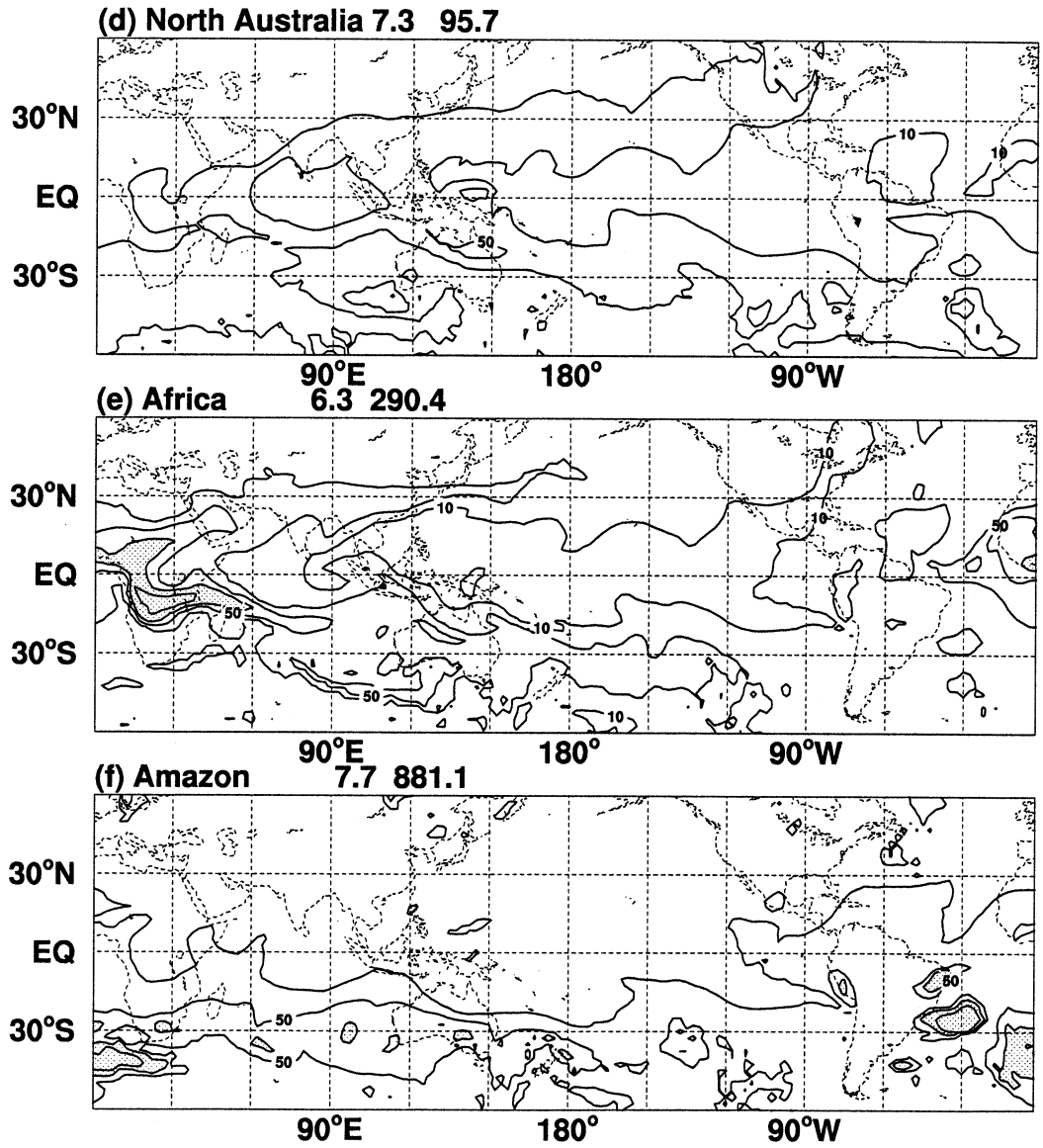


*Fig. 9.* Simulated CO concentration at 250 hPa as a function of longitude and latitude at 06 UTC on 14 October 1997 for emission sites of Kalimantan (a), Sumatra (b), New Guinea (c), northern Australia (d), Africa (e) and the Amazon (f). Contours are 10, 20, 50, 100, 200 ppb. Shaded areas indicate CO concentrations higher than 100 ppb. The E-folding lifetime was 60 days. Detailed simulation conditions are described in Section 3.3.

values and find an optimal combination of parameters which minimize a misfit function. Two types of misfit function were tested; one is maximum of difference (minimax) and the other is a sum of squared difference (least square).

To simplify the analysis, we considered only four parameters, the size of homogeneous background concentrations in the range 20–70 ppb (increments of 0.5), and multiplication factors for emission from Kalimantan, Sumatra and New

Guinea in the range 0–5 (increment of 0.05). Tables 1 and 2 list simulated concentrations so that any other inversion approach may be tested.

These simplifications were based on the following considerations. Although CO from Africa and Amazon had the largest concentrations south of 30°S at 145°E, they did not contribute to peak concentrations from 30°S to 30°N (Fig. 9). The CO concentration from 30°S to 30°N from northern Australia was relatively homogeneous. Estimation of source strength making homogeneous concentrations was unreliable because they could not be distinguished from background concentrations, which consist of emissions from anthropogenic sources, oxidation of methane and non-methane hydrocarbons. We simulated CO concentrations using all sources compiled in the EDGAR dataset (Olivier et al., 1999) with other conditions the same with those of Section 3.4, and found north–south gradients at 250 hPa of the order of 10 ppb (data not shown). North–south gradients of this magnitude were significant for normal background concentrations but were insignificant for the event we were investigating. Therefore, we did not consider these sources. We assumed that OH concentrations were constant during a month and constant within longitude.

Results of the fitting are listed in Table 3. To obtain an emission, factors are to be multiplied by 500 TgC/yr emission rate and duration of emission in units of a fraction of a year. For example if we use one month (31 days) for duration then we obtain 89 TgC for the emission at Kalimantan based on the observation on 14 October with minimax criteria (Section 2.1), although we cannot specify the start and termination of this one month.

Estimated background concentrations ranged from 69.5 to 20 ppb, which is a clear sign of weakness in the solution, since background concentrations were expected to be constant with time. Another weakness was demonstrated in the emissions from Kalimantan and Sumatra. Emissions from Kalimantan were dominated in the minimax and those from Sumatra in least squares (Table 3). This is due to the fact that latitude distributions simulated from Kalimantan and Sumatra were almost proportional (Tables 1 and 2). Results from the minimax were used in the following discussions and those from least squares also deserves the same criticism.

Our estimate for Kalimantan and Sumatra (89 TgC for one month) was significantly larger than the estimate of 32 TgC for August and December estimated from the average of area estimates made from SPOT satellite images (Levine, 1999). The uncertainty in this estimate was reported as 50%. Our estimate therefore exceeded the upper limit of the acceptable range. We have tried to determine the duration of the emissions by using the result of pulse emission experiments, but 2-week observation periods were insufficient to constrain the time evolution of the emissions. We also tried to reduce the duration of the emission. Reduction of duration did not help to reduce total emission because the multiplication factor was increased with the reduction of duration. For example, if the emission period was 10 days, the maximum concentration at 17.5°S, 145°E was 50 ppb at most (Fig. 8a). To fit the

Table 3. *Estimated background and multiplication factor for unit emission of 500 TgC/yr*

| Method | Date | Background | Kalimantan | Sumatra | New Guinea |
|---|---|---|---|---|---|
| Minimax | 12 Sept | 45.0 | 0.0 | 0.2 | 0.35 |
| | 26 Sept | 61.0 | 0.0 | 1.0 | 0.0 |
| | 14 Oct | 20.5 | 2.1 | 0.05 | 0.1 |
| | 28 Oct | 20.0 | 2.5 | 0.7 | 0.1 |
| | 6 Nov | 69.5 | 0.0 | 1.15 | 0.0 |
| | 20 Nov | 61.5 | 0.65 | 0.75 | 0.35 |
| Least squares | 12 Sept | 33.5 | 0.0 | 0.35 | 0.5 |
| | 26 Sept | 59.0 | 0.0 | 0.8 | 0.15 |
| | 14 Oct | 20.0 | 0.0 | 2.1 | 0.1 |
| | 28 Oct | 20.0 | 0.0 | 3.2 | 0.15 |
| | 6 Nov | 69.5 | 0.0 | 1.15 | 0.0 |
| | 20 Nov | 50.5 | 1.75 | 0.15 | 0.65 |

observed 291 ppb (Table 1), the multiplication factor may be larger than 5 if we assume 40 ppb as background concentration.

A chemical feedback for OH concentrations in a dense CO atmosphere is a possible problem in the simplification of the chemical reactions in the CTM. In the dense CO area, OH may be consumed completely, resulting in a longer lifetime of CO. To evaluate the effects of possible low concentration of OH at dense CO areas, we simulated CO with removal of all OH at the lowest two levels. CO concentrations at 250 hPa in this case were increased by 20% at most. This effect possibly reduced the emission estimate by about 20%, although 20% is not enough to fit our estimate to that of Levine (1999).

There are three possible problems in the transport for overestimation. First, related to the horizontal resolution of the CTM, rising motions were treated at a horizontal resolution of 2.5°, although the actual transport occurred on a much smaller scale and the transport of tracers depended on the flow inside an area of 2.5°. Although the amount of CO transported at different angles from that 'gushing' point depends on the detailed distributions of CO inside the lifting tower, we eliminated horizontal structure inside large-scale grid cells. Once the concentrations are mixed inside a lifting tower, information about the detailed structures is lost (Fig. 10). Therefore, we cannot accurately determine the angular dependency of the concentrations in the outflow from the gushing point. Second, related to transport from the gushing point, errors in angular distribution at that point were expanded in a large area. In this study, the relative strength of two branches, one over the north west Pacific and the other over northern Australia, was problematic. Third, related to the accuracy of the wind data, was as follows: in the upper troposphere above the cruise level of commercial aircraft that provide the wind data, wind velocities were estimated by using cloud tracking, but cloud-motion data were not available in the subsidence area. Therefore, winds in the cloud-free area were calculated from the Numerical Weather Prediction model (NWP). For the NWP, subsidence has lower priority or attracts less attention than other areas, because weak subsidence is not associated with severe weather. Therefore, the data we used might have been less accurate in subsidence regions.

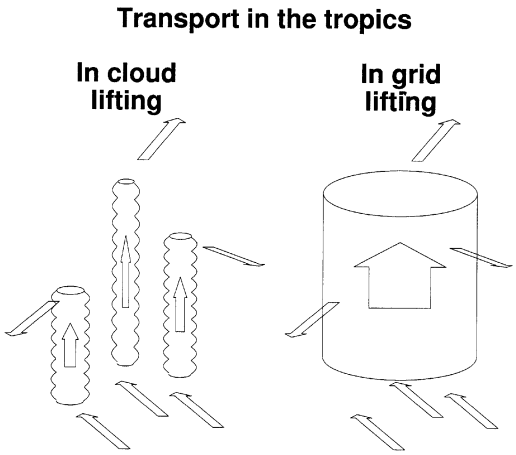


*Fig. 10.* A schematic view of vertical transport in the tropics. Deep cumulus convection lifts air from the ground to upper troposphere. The horizontal size of cloud is an order of 1 km and the interval of grid is an order of 250 km. Deep cumulus convection is standing isolated from others and the horizontal mixing in cloud ensemble is not complete. In the transport model, even if the large-scale convergence and divergence are consistent with the observations, compositions in the outflow from cumulus ensemble are well mixed.

### *3.6. Comparison with independent measurements*

To evaluate our estimates from an independent viewpoint, we used short-term observation data on 23 October (Sawa et al., 1999). Figure 11 shows vertical profiles of observation on 23 October and simulation results at four grid points surrounding a sampling area using an emission estimate based on 28 October. Observed concentrations on 23 October were used for proxy observations on 13 October because the transport time between Kalimantan and the sampling point was estimated as 15 days (Fig. 8). The emission on 23 October at Kalimantan contributed most at sampling point on 7 November, while emission estimate based on 6 November was zero at Kalimantan (Table 3). Although the results were inconsistent, comparison of simulation and the vertical profiles were invaluable for the emission estimate.

Measurement at 1 km was almost 10 ppm, which was as high as CO concentrations in automobile in metropolitan area (Flachsbart, 1999). Simulated concentrations below 1 km were sensitive to height of PBL and the source locations.

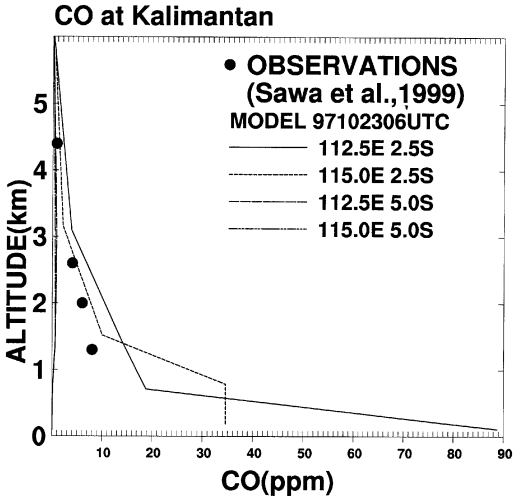


*Fig. 11.* Observed and simulated CO concentrations on 23 October 1997. Lines indicate vertical profiles at four grid points surrounding the sampling point, and dots indicate the mean concentrations by aircraft observations. Emission estimates were based on the observations on 28 October 1997.

Two simulation profiles (112.5°E, 5°S; 115°E, 5°S) off the source were less than 1 ppm, while on the source, concentrations were extremely high at the lowest levels, (two levels at 115°E, 2.5°S, and one level at 112.5°E, 2.5°S). Unfortunately, CO concentrations representative in the PBL were not available for the periods we studied.

Although the vertical gradient of the simulated CO level at 112.5°E, 2.5°S was consistent with the observations, this comparison suggested that the emission estimate was too large. We suspected that the inversion calculation failed to make a correct partitioning between Kalimantan and Sumatra. Also, the PBL thickness estimated in this study might be lower than the real atmosphere, because a thick haze layer was observed up to 4 km (Sawa et al., 1999).

## 4. Summary

The major results are summarized as follows.

1. In October 1997, measured circulations in the Indonesian archipelago were characterized by subsidence south of the equator and concentrated convections west of Sumatra Island. Vertical lifting of materials released from the surface was largely determined by the location of large-scale rising motions, such as a lifting tower, presumably caused by a cloud ensemble.

2. CO distribution patterns due to biomass-burning emissions from the southeast Asian regions of Sumatra, Kalimantan and New Guinea were studied by carrying out simulations using the NIRE-CTM-96 model. The simulated patterns for these regions differed from those for other tropical biomass-burning regions, such as South America and southern Africa, indicating that the biomass burning from southeast Asia was mainly responsible for the large increase in CO in the upper troposphere during 1997.

3. Significant concentrations were distributed over a much wider region in the upper troposphere than at the surface level. Transport from the Indonesia archipelago favored the formations of large-scale anvil and upper tropospheric maximum (UTM).

4. Average time required for transport of surface emissions in the Indonesian archipelago to the air-sampling location of high CO concentration (17.5°S, 145°E, 250 hPa) was about 15 days.

5. mission strength during September to October 1997 was estimated roughly 1000 TgC/yr for Kalimantan Island. The estimate of emissions from Kalimantan were considered higher than acceptable upper limits.

6. Omission of chemical reactions in the CTM was a possible cause of the overestimate while CO–OH feedback alone did not solve the overestimate.

7. Overestimate of source strength might be attributable to insufficient horizontal and vertical resolution of the CTM, the divergent flow at the upper troposphere experienced along the transport from the source to the receptor, and insufficient quality of the wind data.

## 5. Acknowledgements

Airborne CO measurements were made from commercial airliners through a Japanese cooperative program supported by the Meteorological Research Institute in Japan, Japan Airlines (JAL), the JAL Foundation, the Japan Meteorological Agency, and the Japanese Ministry of Transportation. We thank the many crew members

and the ground operation staff of JAL for their kind cooperation in doing the air-sampling measurements. The aircraft observation program was supported financially by the JAL Foundation.

## REFERENCES

Allen, D. J., Kasibhatla, P., Thompson, A. M., Rood, R. B., Doddridge, B. G., Pickering, K. E., Hudson, R. D. and Lin, S.-J. 1996. Transport-induced internannual variability of carbon monoxide determined using a chemistry and transport model. *J. Geophys. Res.* **101**, 28,655–28,669.

Andreae, M. O. 1991. Biomass burning :its history,use, and distribution and its impact on environmental quality and global climate. In: *Atmospheric, climatic, and biospheric implications.* MIT Press, 3–21.

Bergamaschi, P., Hein, R., Brenninkmeijer, C. A. M. and Crutzen, P. 2000. Inverse modeling of the global CO cycle,1, Inversion of CO mixing ratios. *J. Geophys. Res.* **105**, 1909–1927.

Crutzen, P. J. and Andreae, M. O. 1990. Biomass burning in the tropics: Impact on atmospheric chemistry and biogeochemical cycles. *Nature* **250**, 1670–1678.

DeMore, W. B., Sander, S. P., Golden, D. M., Hampson, R. F., Kurylo, M., Howard, C. J., Ravishankara, A. R., Kolb, C. E. and Molina, M. J. 1997. *Chemical kinetics and photochemical data for use in stratospheric modeling*. Technical Report 97–4, Jet Propulsion Laboratory, Pasadena, CA.

Denning, A. S., Holzer, M., Gurney, K. R., Heimann, M., Law, R. M., Rayner, P. J., Fung, I. Y., Fan, S.-M., Taguchi, S., Friendlingstein, P., Balkanski, Y., Taylor, J., Maiss, M. and Levin, I. 1999. Three-dimensional transport and concentration of $SF_6$, a model intercomparison (TransCom 2). *Tellus* **51B**, 266–297.

Dentener, F., Feichter, J. and Jeuken, A. 1999. Simulation of the transport of Rn222 using on-line and off-line global models at different horizontal resolutions: a detailed comparison with measurements. *Tellus* **51B**, 573–602.

Flachsbart, P. 1999. Human exposure to carbon monoxide from mobile sources. *Chemosphere–Global Change Science* **1**, 301–329.

Gregory, D., Morcrette, J.-J., Jakob, C. and Beljaars, A. 1998. Introduction of revised parameterization of physical processes into the IFS. *ECMWF Newsletter* **79**, 2–7.

Gutman, G., Csiszar, I. and Romanov, P. 2000. Using NOAA/AVHRR products to monitor El Niño impacts. Focus on Indonesia in 1997–98. *Bull. Am. Meteorol. Soc.* **81**, 1189–1205.

Hao, W. M. and Liu, M.-H. 1994. Spatial and temporal distribution of tropical biomass burning. *Global Biogeochem. Cycles* **8**, 495–503.

Hoinka, K. P. 1998. Statistics of the global tropopause pressure. *Mon. Weather Rev.* **126**, 3303–3325.

Jonquières, I. and Marenco, A. 1998. Redistribution by deep convection and long-range transport of CO and $CH_4$ emissions from the Amazon basin, as observed by the airborne campaign TROPOZII during the wet season. *J. Geophys. Res.* **103**, 19075–19091.

Kita, K., Fujiwara, M. and Kawakami, S. 2000. Total ozone increase associated with forest fires over the Indonesian region and its relation to the El Niño-Southern oscillation. *Atmos. Environ.* **34**, 2681–2690.

Kritz, M. A., Rosner, S. and Stockwell, D. 1998. Validation of an off-line three-dimensional chemical transport model using observed radon profiles, 1. observations. *J. Geophys. Res.* **103**, 8425–8432.

Lelieveld, J., Crutzen, P. J., Ramanathan, V., Andreae, M. O., Brenninkmeijer, C. A.M., Campos, T., Cass, G. R., Dickerson, R. R., Fischer, H., de Gouw, J. A., Hansel, A., Jefferson, A., Kley, D., de Laat, A. T. J., Lal, S., Lawrence, M. G., Lobert, J. M., Mayol-Bracero, O. L., Mitra, A. P., Novakov, T., Oltmans, S. J., Prather, K. A., Reiner, T., Rodhe, H., Scheeren, H. A., Sikka, D. and Williams, J. 2001. The Indian ocean experiment: widespread air pollution from south and southeast Asia. *Science* **291**, 1031–1036.

Levine, J. S. 1999. The 1997 fires in Kalimantan and Sumatra, Indonesia: gaseous and particulate emissions. *Geophys. Res. Lett.* **26**, 815–818.

Mahowald, N. M., Rasch, P. J., Whittlestone, S. and Prinn, R. G. 1997. Transport of radon-222 to remote troposphere using the model of atmospheric transport and chemistry and assimilated winds from ECMWF and the National Centre for Environmental Predictions/NCAR. *J. Geophys. Res.* **102**, 28,139–28,151.

Maiha, S. 1998. Review of in-country activities related to regional smoke and haze in Papua New Guinea. In: *WMO workshop on regional transboundary smoke and haze in south Asia* (ed. G. R. Carmichael), vol. 2. World Meteorological Organization, Switzerland, 145–175.

Matsueda, H. and Inoue, H. Y. 1996. Measurements of atmospheric $CO_2$ and $CH_4$ using a commercial airline from 1993 to 1994. *Atmosph. Environ.* **30**, 1647–1655.

Matsueda, H., Inoue, H. Y., Ishii, M. and Tsutsumi, Y. 1999. Large injection of carbon monoxide into the upper troposphere due to intense biomass burning in 1997. *J. Geophys. Res.* **104**, 26 867–26 879.

Matsueda, H., Inoue, H. Y., Sawa, Y. and Tsutsumi, Y. 1998. Carbon monoxide in the upper troposphere over the western Pacific between 1993 and 1996. *J. Geophys. Res.* **103**, 19,093–19,110.

Nakajima, T., Higurashi, A., Takeuchi, N. and Herman, J. R. 1999. Satellite and ground-based study of optical properties of 1997 Indonesian forest fire aerosols. *Geophys. Res. Lett.* **26**, 2421–2424.

Newell, R. E., Zhu, Y., Browell, E. V., Read, W. G. and Waters, J. W. 1996. Walker circulation and tropical

upper tropospheric water vapor. *J. Geophys. Res.* **101**, 1961–1974.

Olivier, J. G., Bloos, J. P. J., Berdowski, J. J., Visschedijk, A. J. and Bouwman, A. F. 1999. A 1990 global emission inventory of anthropogenic sources of carbon monoxide on $1^\circ \times 1^\circ$ developed in the framework of EDGAR/GEIA. *Chemosphere–Global Changes Sci.* **1**, 1–17.

Ramonet, M., Roulley, J., Bousquet, P. and Monfray, P. 1996. Radon-222 measurements during the Tropoz II campaign and comparison with a global atmospheric transport model. *J. Atmos. Chem.* **23**, 107–136.

Rayner, P. J. and Law, R. M. 1995. *A comparison of modelled responses to prescribed $CO_2$ sources.* CSIRO Div. of Atmos. Res. Tech. Paper No. 36, 84 pp.

Sawa, Y., Matsueda, H., Tsutsumi, Y., Jensen, T. B., Inoue, H. Y. and Makino, Y. 1999. Tropospheric carbon monoxide and hydrogen measurements over Kalimantan in Indonesia and northern Australia during October, 1997. *Geophys. Res. Lett.* **26**, 1389–1392.

Spivakovsky, C., Logan, J., Montzka, S., Balkanski, Y., Foreman-Fowler, M., Jones, D., Horowitz, L., Fusco, A., Brenninkmeijer, C., Prather, M., Wofsy, S. and Mcelroy, M. 2000. Three-dimensional climatological distribution of tropospheric OH: update and evaluation. *J. Geophys. Res.* **105**, 8931–8980.

Stockwell, D., Kritz, M., Chipperfield, M. and Pyle, J. A. 1998. Validation of an off-line three-dimensional chemical transport model using observed radon profiles, 2. model results. *J. Geophys. Res.* **103**, 8433–8445.

Taguchi, S. 1996. A three-dimensional model of atmospheric $CO_2$ transport based on analyzed winds: model description and simulation results for TRANSCOM. *J. Geophys. Res.* **101**, 15,099–15,109.

Tarantola, A. 1987. *Inverse problem theory: methods for data fitting and model parameter estimation.* Elsevier, Amsterdam, 613 pp.

Thompson, A. M., Witte, J. C., Hudson, R. D., Guo, H., Herman, J. R. and Fujiwara, M. 2001. Tropical tropospheric ozone and biomass burning. *Science* **291**, 2128–2132.

Tiedke, M. 1989. A comprehensive mass flux scheme for cumulus parameterization in large-scale models. *Mon. Weather Rev.* **117**, 1779–1800.

Toma, T., Marjenah, and Hastaniah, 2000. Climate in Bukit Soehrto, East Kalimantan. In: *Rainforest ecosystems of East Kalimantan: El Niño, drought, fire and human impacts* (ed. Guhardja et al.), Ecological Studies Vol. 140. Springer-Verlag, Tokyo, 13–27.

Undén, P. 1989. Tropical data assimilation and analysis of divergence. *Mon. Weather Rev.* **117**, 2495–2517.

Zaucker, F., Daum, P. H., Wetteraucer, U., Berkowitz, C., Kromer, B. and Broecker, W. S. 1996. Atmospheric $^{222}$Rn measurements during the 1993 NARE intensive. *J. Geophys. Res.* **101**, 29,149–29,164.